Comparison of UPFC, SVC and STATCOM in Improving Commutation Failure Immunity of LCC-HVDC Systems

YUNKAI LEI[1], (Member, IEEE), TING LI[1], QUAN TANG[1], YUNLING WANG[1], CHUAN YUAN[2], XIAOXI YANG[3], AND YANG LIU[4], (Member, IEEE)

[1]State Grid Sichuan Economic Research Institute, Chengdu 610000, China
[2]State Grid Sichuan Electrical Power Company, Chengdu 610000, China
[3]College of Economics and Management, Southwest Petroleum University, Chengdu 610500, China
[4]School of Electric Power Engineering, South China University of Technology, Guangzhou 510640, China

Corresponding author: Yang Liu (epyangliu@scut.edu.cn)

ABSTRACT This paper compares the performance of unified power flow controllers (UPFCs), static var compensators (SVCs), and static compensators (STATCOMs) in commutation failure immunity (CFI) improvement of line-commutated converter-based high-voltage direct-current transmission (LCC-HVDC) systems. Theoretical analysis is presented to investigate the capacity requirements of SVCs, STATCOMs, and UPFCs to maintain the inverter-side ac voltage in the cases where three-phase faults occur on the receiving-end ac grids with different short-circuit ratio (SCR). Simulation studies were undertaken to validate the CFI improving performance achieved by UPFCs in comparison to SVCs and STATCOMs. Results of three-phase and single-phase fault tests manifest the superior CFI of LCC-HVDC systems having UPFCs installed.

INDEX TERMS Commutation failure immunity, FACTS, LCC-HVDC, UPFC.

I. INTRODUCTION

LCC-HVDC systems are widely used in the cases of long-distance and large-capacity transmission due to its relative low cost and mature operating and manufacturing techniques [1], [2]. Due the line voltage-based commutating of the thyristor converters, commutation failures (CFs), caused by voltage distortions and voltage magnitude drops of receiving-end ac power grids, are the most challenging problem of concern in LCC-HVDC systems [3]–[5]. Along with the rapid development of distributed energy generations, the receiving-end ac power grids are faced with more randomness and uncertainties [6]–[8]. The variation of wind and solar power leads to more fluctuation in the phase and magnitude of ac voltages [9]–[12], which increases the possibility of CFs in LCC-HVDC inverter stations.

FACTS devices, such as SVCs and STATCOMs, have been widely used in weak ac grids supplied by LCC-HVDC systems to improve the CFI of LCC-HVDC systems [13].

The associate editor coordinating the review of this manuscript and approving it for publication was Huai-Zhi Wang.

Reference [14] investigated the coordination between LCC-HVDC systems and STATCOMs for CFI improvement. Reference [15] compared the CFI improvement achieved by SVCs, synchronous compensators, and fixed capacitors in LCC-HVDC systems. Results of [15] showed that SVCs have the fastest response for load rejection type over-voltage, but can cause serious problems during the recovery of under-voltage caused by single-phase faults. Reference [16] investigated the CFI of LCC-HVDC systems having SVCs and STATCOMs implemented, respectively, results of which suggested that STATCOMs have superior CFI improving performance than SVCs due to their higher response speed. Reference [17] proposed a reactive compensation method for CFI improvement by connecting inductive filters to the windings of converter transformers of LCC-HVDC systems.

Besides the above reactive power compensation-based strategies, CFI improvement of LCC-HVDC systems was also realized with the combination of novel direct-current controllers and CF detection algorithms [18]–[20]. The key idea of the novel control-based methods presented in [18]–[20] is reducing the dc-current order of the
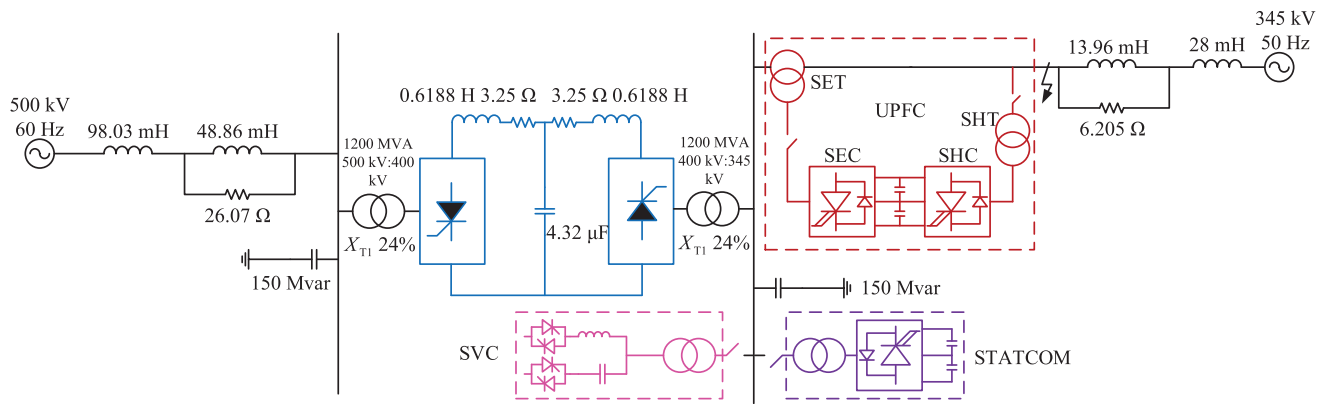
FIGURE 1. The single line circuit diagram of the LCC-HVDC system studied.

LCC-HVDC system once a single-phase or a three-phase fault, which may cause CFs on the inverter station, is detected. Therefore, CFI improvement realized by novel control-based methods [18]–[20] is at the cost of decreasing the power transmission capability of the LCC-HVDC system during the fault process. The advantage of this kind of methods is that they do not require additional hardware investment. Reference [21] investigated the CFI improvement achieved by UPFCs in LCC-HVDC systems, and detailed comparisons between the UPFC-based CFI improving strategy and the novel control-based CFI improving strategies were presented therein. The results of [21] showed that the UPFC-based strategy has superior CFI improving performance than the novel control-based methods in both single-phase and three-phase fault tests.

To provide a comprehensive evaluation of the performance of UPFCs in improving the CFI of LCC-HVDC systems, this paper is dedicated to comparing UPFCs, SVCs and STATCOMs in aspects of capacity requirements and CFI improving performance, respectively. Overall, this paper is organized as follows. Section II introduces the LCC-HVDC system studied in this paper and the control system of an UPFC, which realizes series voltage injection for CFI improvement with the UPFC. Section III evaluates the capacity requirements of SVCs, STATCOMs, and UPFCs in the cases of the receiving-end ac grid with different strength and different kinds of external faults. In Section IV, simulation studies were undertaken on the system introduced in Section II-A and cases of single-phase and three-phase faults were studied. Based on the simulation results, conclusions are presented in Section V.

II. LCC-HVDC SYSTEM STUDIED AND SERIES VOLTAGE INJECTION CONTROL SYSTEM OF UPFCs
A. DESCRIPTION OF THE LCC-HVDC SYSTEM STUDIED
The LCC-HVDC system studied in this paper is as illustrated in Fig. 1. A 1000 MW (500 kV, 2 kA) LCC-HVDC system is utilized to transmit power from a 500 kV, 60 Hz grid to a 345 kV, 50 Hz grid. The rectifier and inverter stations of the LCC-HVDC system are 12-pulse thyristor-based bridges, which are made up of two 6-pulse bridges in Y-connection and Δ-connection, respectively, and thus referred to as
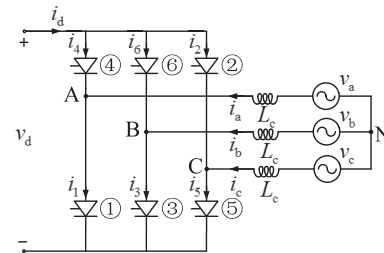

FIGURE 2. The layout of the inverter-side circuit of a LCC-HVDC system.

bridge-Y and bridge-Δ, respectively. Parameters of the system are presented in Fig. 1. To reduce the frequency of CFs on the inverter station, SVCs and STATCOMs are conventionally connected on the inverter-side ac bus to regulated the bus voltage as shown in Fig. 1. The UPFC was normally employed for power flow control of transmission lines. According to the investigation of [21], the UPFC with a novel control system can be employed to inject three-phase voltages in series with the receiving-end ac grid. By implementing an UPFC outside the inverter bus as presented in Fig. 1, the distortion of voltage waveforms of the receiving-end ac grid can be compensated by the three-phase voltages injected by the series converter (SEC) of the UPFC. Then the magnitude drop and distortion of the inverter-side ac voltage can be mitigated in the cases where external disturbances occur in the receiving-end ac grid. The schematic of the series voltage injection control system of the UPFC designed in [21] is as illustrated in Fig. 5. To help understanding, a brief introduction to the control system is presented in the following.

B. MECHANISM OF COMMUTATION FAILURE OF LCC-HVDC SYSTEMS
CFs normally happen on the inverter station of a LCC-HVDC system [22]. The basic module of the inverter station is the thyristor valve-based three-phase full-wave bridge illustrated in Fig. 2. Fig. 3 presents the dc voltage wave shapes and the valve conduction periods of the full-wave bridge, where α denotes the ignition delay angle, β represents the ignition advance angle, μ is the overlap, and γ denotes the extinction advance angle. The transfer of current from one valve to another in the same row of the bridge is referred
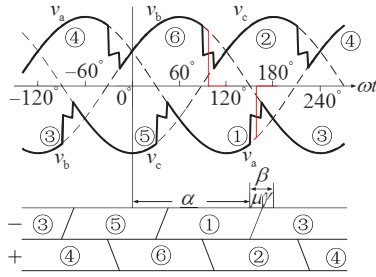
FIGURE 3. Dc voltage wave shapes and valve conduction periods of an inverter station.
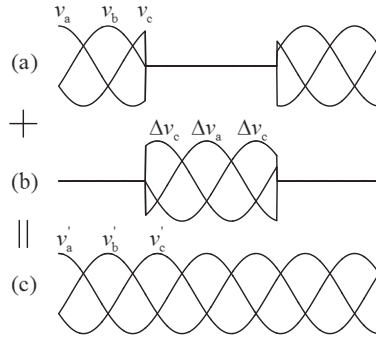

FIGURE 4. Illustration of the mechanism of voltage waveform compensation realized with an UPFC.

to as commutation. Commutation can be accomplished successfully on condition that the changeover from the outgoing valve to the incoming valve is complete before the commutating voltage becomes negative. As pointed out by many existing studies [22], CFs may occur owing to increased direct current, late ignition, or low ac voltage. Among these causes, direct current and ignition of valves are controllable in most cases. In contrast, CFs caused by low ac voltage have not been effectively regulated in practice.

Taking the commutation from valve ① to valve ③ as an example, the commutation starts from $\omega t = \alpha$ as shown in Fig. 3. Due to the inductance L_c of the ac source, there exists an overlap angle μ and the commutation is finished at $\omega t = \alpha + \mu$. For the de-ionization of valves, there is a minimum extinction advance angle limit $\gamma_{\min}$ on γ. Therefore, any magnitude decrease or waveform distortion of v_a, which makes commutation voltage v_{ba} negative on the interval $\omega t \in [\alpha, \alpha + \mu + \gamma_{\min}]$ as marked by the red line in Fig. 3, may lead to a CF of valve ①. With respect to the case of upper row valves, taking the commutation from valve ⑥ to valve ② as an instance, the magnitude decrease or waveform distortion of v_b which makes the commutation voltage v_{cb} positive may result in a CF of valve ⑥ as marked by the red line in Fig. 3. Therefore, system disturbances, which make the commutation voltage negative for lower row valves or positive for upper row valves, may result in CFs on the inverter station.

For disturbed three-phase voltages v_a, v_b, and v_c measured at the inverter-side ac bus presented in Fig. 4 (a), if three-phase voltages Δv_a, Δv_b, and Δv_c shown in Fig. 4 (b) are injected in series with v_a, v_b, and v_c, then the drop of v_a,

v_b, and v_c can be compensated and three-phase voltages like v'_a, v'_b, and v'_c presented in Fig. 4 are provided for the inverter station. In this way, the magnitude decrease and waveform distortion of the inverter-side ac voltages caused by external disturbances, such as phase-to-ground faults, generation trips, and load switches, are effectively compensated and the CFI of the LCC-HVDC system is improved. In order to inject separate three-phase voltages Δv_a, Δv_b, and Δv_c in series with the receiving-end ac source, an UPFC is employed and connected outside the inverter station of the LCC-HVDC system.

C. SERIES VOLTAGE INJECTION CONTROL SYSTEM OF UPFCs

The desirable three-phase voltages v'_{a2}, v'_{b2}, and v'_{c2} for the inverter station are

$$\begin{cases} v'_{a2} = V_{2\_ref}\sin(\omega t) \\ v'_{b2} = V_{2\_ref}\sin(\omega t - \frac{2\pi}{3}) \\ v'_{c2} = V_{2\_ref}\sin(\omega t + \frac{2\pi}{3}) \end{cases} \tag{1}$$

where V_{2_ref} is the magnitude reference of the inverter-side ac voltage, ωt is the phase angle of v_{a1} measured with a phase-locked loop (PLL), and v_{a1}, v_{b1}, and v_{c1} are the three-phase voltages measured at the grid-side terminal of the shunt transformer (SHT) of the UPFC as shown in Fig. 5. The reference Δv_a, Δv_b, and Δv_c of the three-phase voltages injected by the SEC through the series transformer (SET) is

$$\begin{cases} \Delta v_a = v'_{a2} - v_{a1} \\ \Delta v_b = v'_{b2} - v_{b1} \\ \Delta v_c = v'_{c2} - v_{c1} \end{cases} \tag{2}$$

After an abc-dq transformation, the d-axis component Δv_d and q-axis component Δv_q of Δv_a, Δv_b, and Δv_c are obtained. With

$$\begin{cases} \Delta V = \sqrt{\Delta v_d^2 + \Delta v_q^2} \\ \alpha = \arctan\left(\frac{\Delta v_q}{\Delta v_d}\right) \end{cases} \tag{3}$$

and

$$\sigma = 2\arcsin\left[\frac{8\sqrt{2}\pi \, \Delta V V_{dc} V_{1\_LL}}{\sqrt{3}}\right] \tag{4}$$

all four parameters σ, α, ωt, and $\Delta\alpha$ required by the firing pulses generator (FPG) are obtained.

Then the firing pulses Q_1, Q_2, Q_3, and Q_4 generated for the bridge arm of phase A are

$$Q_2 = \text{Mod}[0.5(\pi - \sigma) + \omega t + \alpha + \Delta\alpha, 2\pi] \geq 0 \tag{5}$$
$$\wedge \, \text{Mod}[0.5(\pi - \sigma) + \omega t + \alpha + \Delta\alpha, 2\pi] < 2\pi - \sigma \tag{6}$$
$$Q_3 = \text{Mod}[\omega t + \alpha - \Delta\alpha - 0.5(\pi + \sigma), 2\pi] \geq 0 \tag{7}$$
$$\wedge \, \text{Mod}[\omega t + \alpha - \Delta\alpha - 0.5(\pi + \sigma), 2\pi] < 2\pi - \sigma \tag{8}$$
$$Q_1 = \text{NOT}(Q_3), \quad Q_4 = \text{NOT}(Q_2) \tag{9}$$

where $\wedge$ is logic operator "and", and $\Delta\alpha = 0$. Firing pulses are generated for phase B and phase C with (5) by replacing ωt with $\omega t - \frac{2\pi}{3}$ and $\omega t + \frac{2\pi}{3}$, respectively.
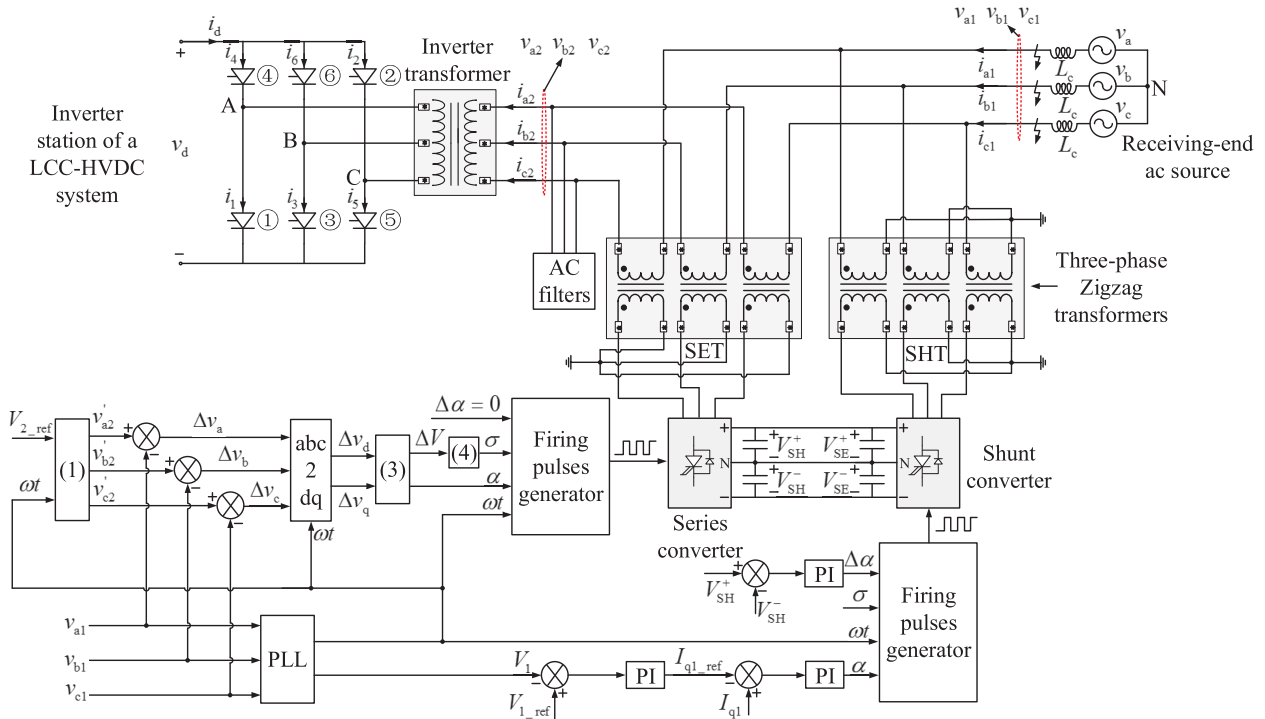
FIGURE 5. The series voltage injection control system of UPFCs.

Pulses generated by the FPG are sent to GTO-based 48-pulse three-level bridges of the SEC as illustrated in Fig. 5. V_{1_LL} is the line-to-line voltage calculated with v_{a1}, v_{b1}, and v_{c1}, and V_{dc} is the dc-link voltage of the UPFC.

III. CAPACITY REQUIREMENTS OF UPFCs, SVCs, AND STATCOMs FOR CFI IMPROVEMENT OF LCC-HVDC SYSTEMS

In this section, the capacity requirements of UPFCs, SVCs, and STATCOMs are compared in the scenario of maintaining the inverter-side ac voltage of a LCC-HVDC system when three-phase-to-ground faults occur on the receiving-end ac grid. For the simplicity of analysis, the ac filters connected on the inverter bus are not considered. Moreover, only the most severe disturbance, i.e., three-phase-to-ground faults out of the inverter bus, is considered.

A. POWER FLOW ANALYSIS OF UPFCs FOR CFI IMPROVEMENT

An UPFC achieves CF attenuation by injecting three-phase voltages in series with the receiving-end ac power source such that the magnitude drop and waveform distortion of the receiving-end ac voltage are compensated and the inverter station of the LCC-HVDC system is provided with satisfactory three-phase sinusoidal voltage waveforms. Concerning the LCC-HVDC system is able to control the current injected into the receiving-end ac grid, the inverter station of the LCC-HVDC system can be modelled with a current source. The single line diagram of the LCC-HVDC system having an UPFC installed is as illustrated in Fig. 6, where $\vec{I}_i$ is the equivalent current source representing the inverter station
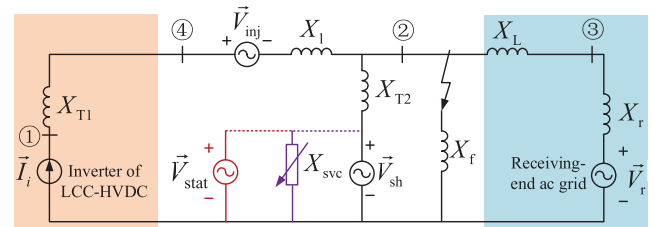

FIGURE 6. The single line circuit diagram of a LCC-HVDC system having an UPFC installed for CF attenuation.

of the LCC-HVDC system, X_{T1} denotes the impedance of the inverter transformer, $\vec{V}_{inj}$ represents the voltage vector injected by the SEC of the UPFC, X_{T2} is the impedance of the SHT of the UPFC, $\vec{V}_{sh}$ denotes the voltage output of the shunt converter (SHC) of the UPFC, X_l represents the leakage impedance of the SET of the UPFC, X_L denotes the impedance of transmission line, X_r represents the equivalent internal impedance of the receiving-end ac grid, $\vec{V}_r$ is the voltage of the receiving-end ac grid, and X_f denotes the three-phase-to-ground fault impedance.

In the cases where no fault occurs in the LCC-HVDC system, i.e., X_f presented in Fig. 6 does not exist, the SEC of the UPFC does not inject voltage into the system and $\vec{V}_{inj} = 0$. Moreover, $\vec{V}_{sh} = \vec{V}_2$ holds, where $\vec{V}_2$ denotes the voltage of node 2 and $\vec{V}_i (i = 1, 3, 4)$ denote the voltage of node 1, 3, and 4, respectively. Therefore, it can be obtained that

$$\begin{cases} \vec{V}_2 = \vec{V}_r + j(X_L + X_r)\vec{I}_i \\ \vec{V}_4 = \vec{V}_r + j(X_L + X_r + X_l)\vec{I}_i \end{cases} \quad (10)$$

When a three-phase-to-ground fault with a fault impedance X_f occurs on the receiving-end ac grid as indicated in Fig. 6, it can be obtained that

$$\begin{cases} \dfrac{1}{jX_{T1}}\vec{V}_1 - \dfrac{1}{jX_{T1}}\vec{V}_4 = \vec{I}_i \\[2mm] -\dfrac{1}{jX_{T1}}\vec{V}_1 + \left(\dfrac{1}{jX_{T1}} + \dfrac{1}{jX_l}\right)\vec{V}_4 = \dfrac{\vec{V}_{inj} + \vec{V}_2}{jX_l} \\[2mm] \left(\dfrac{1}{jX_{T2}} + \dfrac{1}{jX_f} + \dfrac{1}{jX_L}\right)\vec{V}_2 - \dfrac{1}{jX_L}\vec{V}_3 = \vec{I}_i + \dfrac{\vec{V}_{sh}}{jX_{T2}} \\[2mm] -\dfrac{1}{jX_L}\vec{V}_2 + \left(\dfrac{1}{jX_L} + \dfrac{1}{jX_r}\right)\vec{V}_3 = \dfrac{\vec{V}_r}{jX_r} \end{cases} \quad (11)$$

Solving (11), it can be obtained that

$$\vec{V}_2 = \frac{jX_{eq2}\vec{I}_i + X_L X_f(X_L + X_r + X_{T2})\vec{V}_r}{X_{eq1}} \quad (12)$$

where $X_{eq1} = (X_L + X_r)(X_f X_L + X_{T2} X_f + X_{T2} X_L) - X_{T2} X_f X_r$ and $X_{eq2} = X_L X_f \left[X_{T2}(X_L + X_r) + (X_L + X_r)^2 \right]$. If the voltage provided to the inverter station of the LCC-HVDC system is regulated at its pre-fault value despite of the fault, then the voltage $\vec{V}_{inj}$ injected by the UPFC should satisfy $\vec{V}_{inj} = \vec{V}_{40} - \vec{V}_2$, where $\vec{V}_{40}$ is the pre-fault value of $\vec{V}_4$ denoted in (10), then it can be obtained that

$$\vec{V}_{inj} = \vec{V}_r + j(X_L + X_r + X_l)\vec{I}_i - \vec{V}_2 = \vec{V}_{20} + X_l\vec{I}_i - \vec{V}_2 \quad (13)$$

where $\vec{V}_{20}$ is the pre-fault value of V_2. The power flowing through the SET of the UPFC is

$$S_{se} = \vec{V}_{inj}\left(\vec{I}_i\right)^* \quad (14)$$

The SHC of the UPFC is designed to maintain the dc-link voltage of the UPFC and the ac grid voltage. The active power flowing through the SHC equals the active power output of the SEC, and the reactive power flowing through the SHC depends on its reactive power control loop. Then the voltage output of the SHC maintains at its pre-fault value, i.e., $\vec{V}_{sh} = \vec{V}_{20}$. Thus the power flowing through the SHT equals

$$S_{sh} = \vec{V}_{20}\left(\frac{\vec{V}_{20} - \vec{V}_2}{jX_{T2}}\right)^* \quad (15)$$

In the worst case, where the three-phase-to-ground fault is a metallic ground fault, i.e. $X_f \approx 0$, then it has

$$\begin{cases} \lim\limits_{X_f \to 0} S_{se} = \vec{V}_{20}\left(\vec{I}_i\right)^* \\[2mm] \lim\limits_{X_f \to 0} S_{sh} = j\dfrac{|\vec{V}_{20}|^2}{X_{T2}} \end{cases} \quad (16)$$

According to (16), the power flowing through the SET is finite even the inverter-side ac voltage is required to be controlled at its pre-fault value in the worst case where metallic three-phase-to-ground fault occurs. (16) indicates the capacity requirement of the UPFC for CFI improvement of the LCC-HVDC system.

B. POWER FLOW ANALYSIS OF SVCs AND STATCOMs FOR CFI IMPROVEMENT

A SVC is composed of a coupling transformer, thyristor-controlled reactor banks (TCR), and thyristor-switched capacitor banks (TSC) [23]. The phase control of TCR offers a continuous variation of inductive reactive power output, and the switching of TSC allows a discrete variation of the capacitive reactive power output of the SVC. Essentially, the SVC regulates its reactive power input to the external power grid by varying its equivalent admittance [24]. The single line circuit diagram of a LCC-HVDC system having a SVC implemented for CF attenuation is illustrated in Fig. 6, where X_{T2} is the impedance of the coupling transformer of the SVC and X_{svc} denotes the equivalent impedance of the SVC. Before the three-phase-to-ground fault is applied to the system, the voltage of node 2 is the same as that presented in (10).

For the case of SVC, if $\vec{V}_2$ was required to be regulated at its pre-fault value $\vec{V}_{20}$ by the SVC, then it can be obtained that

$$X_{svc} = -X_f - X_{T2} \quad (17)$$

Then the power flowing through the coupling transformer of the SVC is

$$S_{svc} = \vec{V}_{20}\left[\frac{\vec{V}_{20}}{j(X_{T2} + X_{svc})}\right]^* \\ = j\frac{|\vec{V}_{20}|^2}{X_f} \quad (18)$$

In the extreme case where the applied fault is a metallic ground fault, it has

$$\lim\limits_{X_f \to 0} S_{svc} = \infty \quad (19)$$

Therefore, the reactive power required is infinite if $\vec{V}_2$ was required to be regulated at its pre-fault value with the SVC when a metallic fault occurs in the LCC-HVDC system.

A STATCOM is a voltage source converter connected to power grids through a coupling transformer [25], [26]. The active power and reactive power generated by a STATCOM can be regulated by adjusting the phase and magnitude of its voltage, respectively. The single line diagram of a LCC-HVDC system having a STATCOM implemented outside the inverter transformer is as shown in Fig. 6, where X_{T2} denotes the impedance of the coupling transformer of the STATCOM and $\vec{V}_{stat}$ represents the voltage output of the STATCOM. Under normal operating conditions, the voltage of node 2 is the same as that denoted in (10).

For the case of STATCOM, if $\vec{V}_2$ was required to be regulated at its pre-fault value $\vec{V}_{20}$, then the voltage output of the STATCOM should be

$$\vec{V}_{stat} = \frac{(X_{eq1} - X_{T2}X_fX_L)\vec{V}_{20}}{X_fX_L(X_L + X_r)} \quad (20)$$

Then the power flowing through the coupling transformer of the STATCOM is

$$S_{\text{stat}} = j \frac{X_{\text{eq3}} |\overrightarrow{V}_{20}|^2}{X_{\text{T2}} X_{\text{f}}^2 X_{\text{L}}^2 (X_{\text{L}} + X_{\text{r}})^2} \tag{21}$$

where $X_{\text{eq3}} = (X_{\text{eq1}} - X_{\text{T2}} X_{\text{f}} X_{\text{L}})[X_{\text{eq1}} - X_{\text{T2}} X_{\text{f}} X_{\text{L}} - X_{\text{f}} X_{\text{L}} (X_{\text{L}} + X_{\text{r}})]$. In the extreme case where the applied three-phase-to-ground fault is a metallic fault, i.e., $X_{\text{f}} \approx 0$, it has

$$\lim_{X_{\text{f}} \to 0} S_{\text{stat}} = \infty \tag{22}$$

Therefore, the power flowing through the coupling transformer of the STATCOM is infinite in the case where V_2 was required to be controlled at its pre-fault value when a three-phase metallic ground fault occurs on the receiving-end ac system. S_{sat} indicates the capacity requirement of the STATCOM for CFI improvement of the LCC-HVDC system.

C. COMPARISON OF CAPACITY REQUIREMENTS OF UPFCs, SVCs, AND STATCOMs FOR CFI IMPROVEMENT OF LCC-HVDC SYSTEMS

With the parameters of the LCC-HVDC system presented in Section II and neglecting impedances of ac filters connected on the inverter bus, it has $X_{\text{T1}} = 0.02$ $p.u.$, $X_l = 0.05$ $p.u., X_{\text{L}} = 0.0074$ $p.u.$ For the UPFC, $X_{\text{T2}} = 0.1$ $p.u.$ For the SVC, $X_{\text{T2}} = 0.045$ $p.u.$ For the STATCOM, $X_{\text{T2}} = 0.1$ $p.u.$ Let node 3 be the reference bus, then $\overrightarrow{V}_r = 1\angle 0°$ denotes the nominal value of the receiving-end ac grid voltage. In the steady state, the LCC-HVDC system transmits 985 MW active power and 50 Mvar reactive power to the receiving-end ac power grid. Therefore, the current source denoting the inverter station can be written as $\overrightarrow{I}_i = 9.86\angle -2.9°$. X_r describes the strength of the receiving-end ac grid, and it can be calculated with $X_r = \frac{V_r^2}{P_n * \text{SCR}}$, where SCR is the short-circuit ratio of the receiving-end ac grid and P_n denotes the nominal dc power transmitted by the LCC-HVDC system.

According to (14), (15), (18), and (21), to maintain the post-fault voltage of node 4 for UPFC and that of node 2 for SVC and STATCOM, the power flowing though coupling transformers of the SET and the SHT of UPFCs, SVCs, and STATCOMs are shown in Fig. 7 (a), 7 (c), and 7 (e), respectively. It can be seen that the capacity requirement (CR) of the UPFC is the lowest, and the CR of the STATCOM is the highest to achieve the same level of V_2 at different fault levels. When the fault impedance is $X_f = 0.1$ p.u., the CR of the SET of the UPFC is about 3.1 p.u., the CR of the SHT is about 3.8 p.u., the CR of the SVC reaches 14 p.u., whilst the CR of the STATCOM is nearly 28 p.u.

Concerning receiving-end ac grids with different strength, to maintain the inverter-side ac voltage in the cases where a three-phase-to-ground fault with fault impedance $X_f = 0.1$ p.u. occurs on the receiving-end ac grid, the power flowing through coupling transformers of SETs, SHTs, SVCs, and STATCOMs calculated with (14), (15), (18), and (21) are
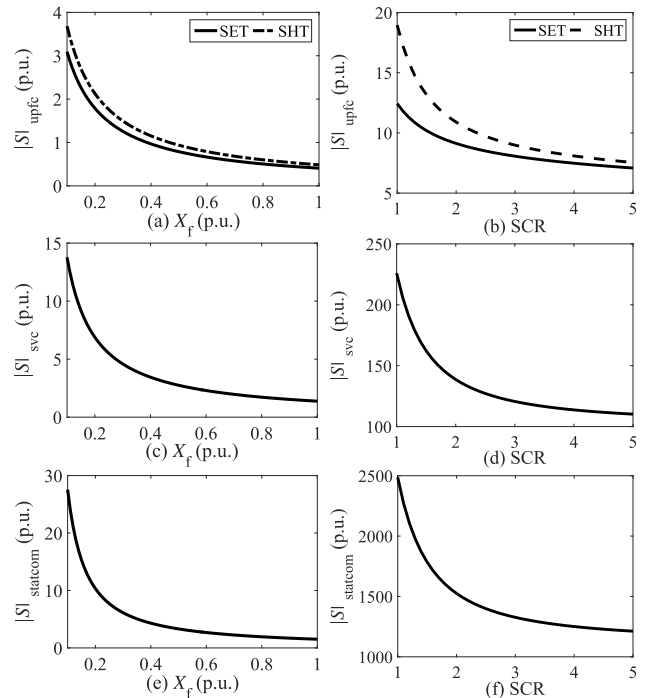

FIGURE 7. Capacity requirements of UPFCs, SVCs, and STATCOMs to maintain V_2 at its pre-fault value in the cases of different X_f and receiving-end ac grids with different SCR.

shown in Fig. 7 (b), 7 (d), and 7 (f), respectively. It can be found that the CR of UPFCs, SVCs, and STATCOMs reduces as the increase of the SCR of the receiving-end ac grid. For the case of SCR=1, the CR of the SET of the UPFC is about 12.5 p.u., and the CR of the SHT is about 19 p.u. In terms of SVC, the CR reaches about 225 p.u. STATCOM shows the highest CR, which reaches 2500 p.u.

IV. SIMULATION STUDIES

Simulation studies were undertaken on the test system introduced in Section II-A. The commutation failure prevention algorithm introduced in [20] was implemented in the test system. Three-phase and single-phase fault tests were carried out to evaluate the CFI of LCC-HVDC systems having an UPFC, a SVC, and a STATCOM installed, respectively. In LCC-HVDC systems having a SVC installed, additional ac filters were implemented to filter the harmonics introduced by the SVC. The commutation failure immunity index (CFII) proposed in [27] was employed to present a qualitative evaluation of the CFI of LCC-HVDC systems. The higher CFII implies the stronger CFI of the LCC-HVDC system.

A. THREE-PHASE-TO-GROUND FAULT TESTS
Three-phase-to-ground faults at the receiving-end ac power grid is a direct cause of the CFs of LCC-HVDC systems. Hence, the CF sensitivity of the test system with and without UPFC implemented respectively was evaluated in the cases of three-phase-to-ground faults. Three-phase-to-ground faults were applied at the fault location indicated in Fig. 1 with fault inductances varied from 0.18 H to 0.39 H in one operation

TABLE 1. Commutation failure sensitivity of the test system with and without UPFC implemented in the cases where three-phase-to-ground faults occurred on the system.

Fault inductance L (H)	Fault time (s)																			
	0.900	0.901	0.902	0.903	0.904	0.905	0.906	0.907	0.908	0.909	0.910	0.911	0.912	0.913	0.914	0.915	0.916	0.917	0.918	0.919
0.39																				
0.38																				
0.37																				
0.36																				
0.35																				
0.34																				
0.33																				
0.32																				
0.31																				
0.30																				
0.29																				
0.28																				
0.27																				
0.26																				
0.25																				
0.24																				
0.23																				
0.22																				
0.21																				
0.20																				
0.19																				
0.18																				
0.00																				

No commutation failure
Commutation failures occurred on the test system without UPFC
Commutation failures occurred on the test system with UPFC

cycle from 0.900 s to 0.919 s. The obtained test results are presented in Table 1. It can be seen that the lowest endurable fault inductance (EFI) achieved by the system without UPFC was 0.37 H, in contrast, the lowest EFI achieved by the system with UPFC was 0.19 H. Meanwhile, at all tested fault time points, the LCC-HVDC system having UPFC implemented showed lower EFI than that without UPFC.

The dynamics of the test LCC-HVDC system, obtained in the case where a three-phase-to-ground fault was applied through a fault inductance $L = 0.13$ H at $t = 1$ s on the receiving-end ac grid with SCR=8.5, are illustrated in Fig. 8. Owning to the three-phase fault, inverter bus ac voltage presented severe magnitude drops in the test LCC-HVDC systems having a 200 MVA SVC and a 300 MVA STATCOM installed, respectively, as illustrated in Fig. 8 (a) and 8 (c). As a consequence, CFs were observed on inverter valves, which is manifested in Fig. 8 (b) and 8 (d). In contrast, attributed to the voltage injected by the UPFC as presented in Fig. 8 (f), the inverter bus ac voltage showed little magnitude drop in the test system having a 100 MVA UPFC implemented, which is depicted in Fig. 8 (e). As such, no CFs were found in the test LCC-HVDC system having the UPFC installed.

B. SINGLE-PHASE-TO-GROUND FAULT TESTS

CFI of the test LCC-HVDC system having different kinds of FACTS devices installed was also evaluated in the cases where single-phase-to-ground faults occurred on the receiving-end ac grid with different SCR at the fault location indicated in Fig. 1. According to the results presented in Fig. 9 (a), the CFI improving performance of SVCs was not satisfactory. Actually, in some cases, the implementation of SVCs made the test system more susceptible to CFs with respect to single-phase faults, such as the cases of SCR=6 and SCR=7 presented in Fig. 9 (a). A 100 MVA UPFC was implemented and the CFII of the test system are illustrated in Fig. 9 (b). It can be seen that the implementation of the
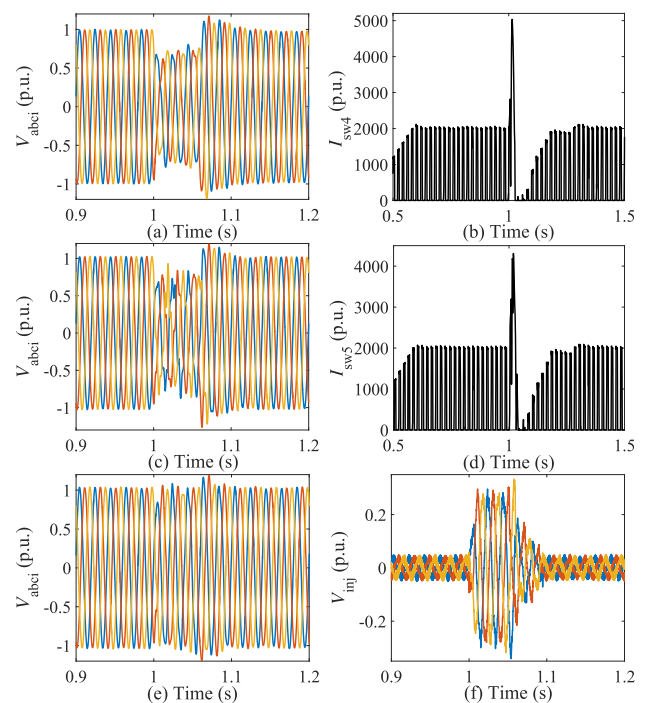

FIGURE 8. Dynamics of the test LCC-HVDC system having a 200 MVA SVC, a 300 MVA STATCOM and a 100 MVA UPFC implemented, respectively, obtained in the case where a three-phase-to-ground fault occurred at $t = 1$ s on the receiving-end ac grid with SCR=8.5 through a fault inductance $L = 0.13$ H ((a) Inverter bus three-phase voltages of the test system having a 200 MVA SVC installed (b) Current of valve 4 of bridge-Y of the inverter station obtained in the test system having a 200 MVA SVC installed (c) Inverter bus three-phase voltages of the test system having a 300 MVA STATCOM installed (d) Current of valve 5 of bridge-Y of the inverter station obtained in the test system having a 300 MVA STATCOM installed (e) Inverter bus three-phase voltages of the test system having a 100 MVA UPFC installed (f) Three-phase voltages injected by the 100 MVA UPFC).

100 MVA UPFC had improved the CFI of the test system dramatically with respect to single-phase faults. Referring to Fig. 9 (c), the implementation of STATCOMs did not help to enhance the CFI of the test system in most cases.
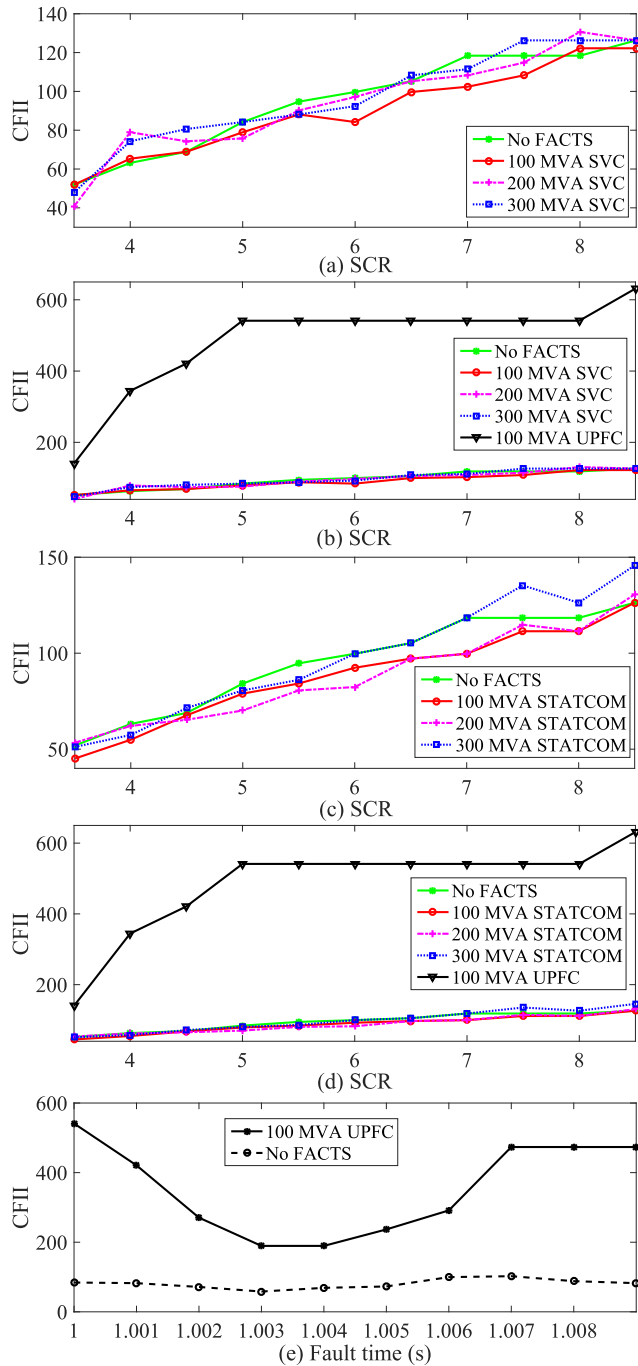
FIGURE 9. CFII of the test LCC-HVDC system obtained in the cases where single-phase-to-ground faults occurred on the receiving-end ac grid with different SCR and single-phase-to-ground faults occurred at different time points on the receiving-end ac grid with SCR=5 ((a) CFII of the test system having a 100 MVA SVC, a 200 MVA SVC, a 300 MVA SVC, and no FACTS device installed, respectively, (b) CFII of the test system having a 100 MVA SVC, a 200 MVA SVC, a 300 MVA SVC, a 100 MVA UPFC, and no FACTS device installed, respectively, (c) CFII of the test system having a 100 MVA STATCOM, a 200 MVA STATCOM, a 300 MVA STATCOM, and no FACTS device installed, respectively, (d) CFII of the test system having a 100 MVA STATCOM, a 200 MVA STATCOM, a 300 MVA STATCOM, a 100 MVA UPFC, and no FACTS device installed, respectively, (e) CFII of the test system having a 100 MVA UPFC and no FACTS device installed respectively obtained in the cases where single-phase-to-ground faults occurred at different time points on the receiving-end ac grid with SCR=5).

In contrast, the CFII of the test system having a 100 MVA UPFC installed was significantly higher than those of the test
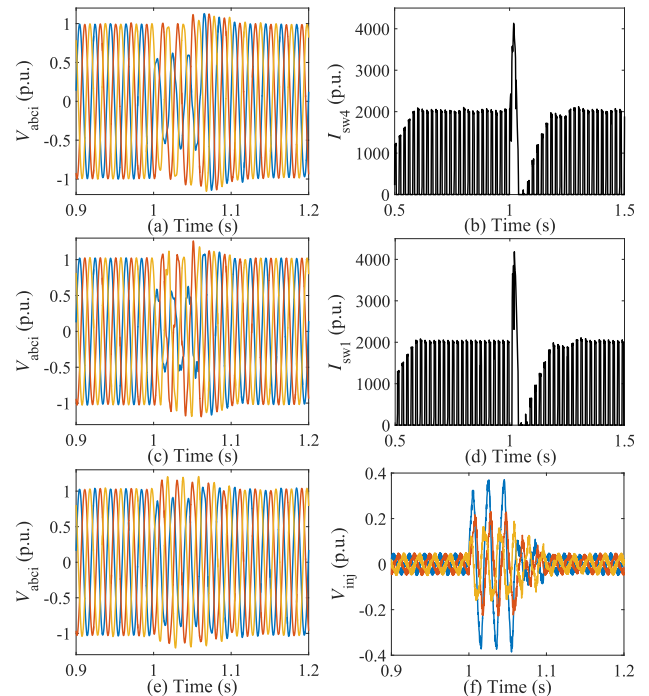

FIGURE 10. Dynamics of the test LCC-HVDC system having a 300 MVA SVC, a 300 MVA STATCOM, and a 100 MVA UPFC implemented, respectively, obtained in the case where a single-phase-to-ground fault occurred at $t = 1$ s on the receiving-end ac grid with SCR=8.5 through a fault inductance $L = 0.06$ H ((a) Inverter bus three-phase voltages of the test system having a 300 MVA SVC installed (b) Current of valve 4 of bridge-Y of the inverter station obtained in the test system having a 300 MVA SVC installed (c) Inverter bus three-phase voltages of the test system having a 300 MVA STATCOM installed (d) Current of valve 1 of bridge-Y of the inverter station obtained in the test system having a 300 MVA STATCOM installed (e) Inverter bus three-phase voltages of the test system having a 100 MVA UPFC installed (f) Three-phase voltages injected by the 100 MVA UPFC).

system having no FACTS or STATCOMs installed, which is manifested by Fig. 9 (d). From the above, it can be found that the test system having no FACTS installed showed superior CFI than those having SVCs or STATCOMs implemented in the cases of single-phase faults. To further evaluate the CFI of the test system with an UPFC installed in single-phase fault tests, the CFII of the test system having a 100 MVA UPFC implemented is presented in Fig. 9 (e) in comparison to the system with no FACTS installed. The results depicted in Fig. 9 (e) were obtained in the cases where single-phase-to-ground faults were applied at different time points from $t = 1$ s to $t = 1.009$ s on the receiving-end ac grid with SCR=8.5. It can be seen that the 100 MVA UPFC improved the CFI of the test system at all tested fault time points.

The dynamics of the test system, obtained in the case where a single-phase-to-ground fault occurred at $t = 1$ s on the receiving-end ac grid with SCR=8.5 through an inductance $L = 0.06$ H, is illustrated in Fig. 10. As depicted in Fig. 10 (a), phase A voltage measured at the inverter bus of the test system having a 300 MVA SVC installed showed severe magnitude drop. Consecutive CFs were observed on valve 4 of bridge-Y of the inverter station of the LCC-HVDC system as illustrated in Fig. 10 (b). For the test LCC-HVDC system having a

300 MVA STATCOM implemented, severe magnitude drop and distortion were also found in the voltage of phase A as presented in Fig. 10 (c). CFs were observed on valve 1 of bridge-Y of the inverter station of the test system, which is shown in Fig. 10 (d). In comparison, the voltage distortion of phase A was effectively compensated by three-phase voltages injected by a 100 MVA UPFC as manifested in Fig. 10 (e). The three-phase voltages injected by the UPFC were depicted in Fig. 10 (f), in which the voltage magnitude of phase A was higher than those of phase B and phase C. As such, the distortion of the receiving-end ac voltage was properly compensated in the test system having a 100 MVA UPFC implemented. As such, no CFs were found in the system.

V. CONCLUSION

This paper has compared the CFI improvement of LCC-HVDC systems having SVCs, STATCOMs, and UPFCs installed, respectively.

According to the analysis of the capacity requirements of different kinds of FACTS devices, to maintain the inverter-side ac voltage, the required capacities of SVCs, STATCOMs, and UPFCs increase as the SCR of the receiving-end ac grid and the fault inductance X_f decrease, respectively. In the cases where the SCR of the receiving-end ac grid approaches zero, namely, the receiving-end ac grid is a passive network, the required capacities of SVCs and STATCOMs, which were expected to maintain the inverter-side ac voltage, increase to infinity. In the cases where the three-phase fault inductance $X_f \approx 0$, namely, the three-phase fault is a metallic fault, the required capacities of SVCs and STATCOMs, which were expected to maintain the inverter-side ac voltage of LCC-HVDC systems, are infinity. By contrast, the capacity requirements of UPFCs in the above two cases are finite. For receiving-end ac grids with the same SCR and three-phase faults with the same fault impedance X_f, the capacity requirement of UPFCs is much lower than those of SVCs and STATCOMs.

In the three-phase fault tests, simulation results suggested that implementing SVCs in the receiving-end ac grids helped to improve the CFI of the test LCC-HVDC systems. With respect to STATCOMs, they improved the CFI of the test LCC-HVDC systems in all the cases tested. Therefore, STATCOMs showed better CFI improving performance than SVCs. In comparison, UPFCs were able to offer better CFI improving performance than both SVCs and STATCOMs in the cases where three-phase faults occurred on the receiving-end ac grids. Moreover, the test LCC-HVDC system with a 100 MVA UPFC showed much higher CFII than those having a 200 MVA SVC and a 300 MVA STATCOM implemented, respectively, in the cases where the fault time varied between 1 s and 1.009 s.

Analogously, in the single-phase fault tests, UPFCs presented much better CFI improving performance than SVCs and STATCOMs. Moreover, the implementation of SVCs and STATCOMs actually have adverse effects on the successful commutation of inverter stations in the cases where single-phase-to-ground faults occurred on receiving-end ac grids. Referring to the dynamics of inverter-side ac voltage and valve currents in both single-phase and three-phase fault tests, the three-phase voltages injected by the UPFC properly compensated the distortion and magnitude drop of the inverter-side ac voltage. Consequently, the frequency of CFs was significantly reduced in the LCC-HVDC systems having UPFCs installed.

REFERENCES

[1] Y. Xue, X.-P. Zhang, and C. Yang, "Commutation failure elimination of LCC HVDC systems using thyristor-based controllable capacitors," *IEEE Trans. Power Del.*, vol. 33, no. 3, pp. 1448–1458, Jun. 2018.

[2] B. Li, J. He, Y. Li, and B. Li, "A review of the protection for the multi-terminal VSC-HVDC grid," *Protection Control Mod. Power Syst.*, vol. 4, no. 3, pp. 239–249, 2019.

[3] C. V. Thio, J. B. Davies, and K. L. Kent, "Commutation failures in HVDC transmission systems," *IEEE Trans. Power Del.*, vol. 11, no. 2, pp. 946–957, Apr. 1996.

[4] X. Fu, Q. Guo, and H. Sun, "Statistical machine learning model for stochastic optimal planning of distribution networks considering a dynamic correlation and dimension reduction," *IEEE Trans. Smart Grid*, vol. 11, no. 4, pp. 2904–2917, Jul. 2020.

[5] X. Fu, H. Chen, P. Xuan, and R. Cai, "Improved LSF method for loss estimation and its application in DG allocation," *IET Gener., Transmiss. Distrib.*, vol. 10, no. 10, pp. 2512–2519, Jul. 2016.

[6] H. Wang, Z. Lei, X. Zhang, B. Zhou, and J. Peng, "A review of deep learning for renewable energy forecasting," *Energy Convers. Manage.*, vol. 198, Oct. 2019, Art. no. 111799. [Online]. Available: http://www.sciencedirect.com/science/article/pii/S0196890419307812

[7] H. Wang, Y. Liu, B. Zhou, C. Li, G. Cao, N. Voropai, and E. Barakhtenko, "Taxonomy research of artificial intelligence for deterministic solar power forecasting," *Energy Convers. Manage.*, vol. 214, Jun. 2020, Art. no. 112909. [Online]. Available: http://www.sciencedirect.com/science/article/pii/S0196890420304477

[8] D. Xu, Q. Wu, B. Zhou, C. Li, L. Bai, and S. Huang, "Distributed multi-energy operation of coupled electricity, heating and natural gas networks," *IEEE Trans. Sustain. Energy*, early access, Dec. 23, 2020, doi: 10.1109/TSTE.2019.2961432.

[9] H.-Z. Wang, G.-Q. Li, G.-B. Wang, J.-C. Peng, H. Jiang, and Y.-T. Liu, "Deep learning based ensemble approach for probabilistic wind power forecasting," *Appl. Energy*, vol. 188, pp. 56–70, Feb. 2017. [Online]. Available: http://www.sciencedirect.com/science/article/pii/S0306261916317421

[10] H. Z. Wang, G. B. Wang, G. Q. Li, J. C. Peng, and Y. T. Liu, "Deep belief network based deterministic and probabilistic wind speed forecasting approach," *Appl. Energy*, vol. 182, pp. 80–93, Nov. 2016. [Online]. Available: http://www.sciencedirect.com/science/article/pii/S0306261916312053

[11] H. Wang, Z. Lei, Y. Liu, J. Peng, and J. Liu, "Echo state network based ensemble approach for wind power forecasting," *Energy Convers. Manage.*, vol. 201, Dec. 2019, Art. no. 112188. [Online]. Available: http://www.sciencedirect.com/science/article/pii/S019689041931194X

[12] Y. Liu, Z. Lin, K. Xiahou, M. Li, and Q. H. Wu, "On the state-dependent switched energy functions of DFIG-based wind power generation systems," *CSEE J. Power Energy Syst.*, vol. 6, no. 2, pp. 318–328, Jun. 2020.

[13] J. Dixon, L. Moran, J. Rodriguez, and R. Domke, "Reactive power compensation technologies: State-of-the-art review," *Proc. IEEE*, vol. 93, no. 12, pp. 2144–2164, Dec. 2005.

[14] C.-K. Kim, "Dynamic coordination strategies between HVDC and STATCOM," in *Proc. Transmiss. Distrib. Conf. Expo., Asia Pacific*, Oct. 2009, pp. 1–9.

[15] O. B. Nayak, A. M. Gole, D. G. Chapman, and J. B. Davies, "Dynamic performance of static and synchronous compensators at an HVDC inverter bus in a very weak AC system," *IEEE Trans. Power Syst.*, vol. 9, no. 3, pp. 1350–1358, Aug. 1994.

[16] J. Burr, S. Finney, and C. Booth, "Comparison of different technologies for improving commutation failure immunity index for LCC HVDC in weak AC systems," in *Proc. 11th IET Int. Conf. AC DC Power Transmiss.*, 2015, pp. 1–7.

[17] Y. Li, L. Luo, C. Rehtanz, S. Rüberg, and F. Liu, "Realization of reactive power compensation near the LCC-HVDC converter bridges by means of an inductive filtering method," *IEEE Trans. Power Electron.*, vol. 27, no. 9, pp. 3908–3923, Sep. 2012.

[18] C. Guo, Y. Liu, C. Zhao, X. Wei, and W. Xu, "Power component fault detection method and improved current order limiter control for commutation failure mitigation in HVDC," *IEEE Trans. Power Del.*, vol. 30, no. 3, pp. 1585–1593, Jun. 2015.

[19] Z. Wei, Y. Yuan, X. Lei, H. Wang, G. Sun, and Y. Sun, "Direct-current predictive control strategy for inhibiting commutation failure in HVDC converter," *IEEE Trans. Power Syst.*, vol. 29, no. 5, pp. 2409–2417, Sep. 2014.

[20] L. Zhang and L. Dofnas, "A novel method to mitigate commutation failures in HVDC systems," in *Proc. Int. Conf. Power Syst. Technol.*, 2002, pp. 51–56.

[21] Q. Chen, Y. Lei, Y. Wang, Y. Su, A. Li, F. Liu, and Y. Liu, "Improving CFI of LCC-HVDC systems through voltage compensation using UPFC," in *Proc. IEEE Innov. Smart Grid Technol.-Asia (ISGT Asia)*, May 2019, pp. 2234–2239.

[22] P. Kundur, N. J. Balu, and M. G. Lauby, *Power System Stability and Control*, vol. 7. New York, NY, USA: McGraw-Hill, 1994.

[23] N. Mithulananthan, C. A. Canizares, J. Reeve, and G. J. Rogers, "Comparison of PSS, SVC, and STATCOM controllers for damping power system oscillations," *IEEE Trans. Power Syst.*, vol. 18, no. 2, pp. 786–792, May 2003.

[24] C. A. Canizares and Z. T. Faur, "Analysis of SVC and TCSC controllers in voltage collapse," *IEEE Trans. Power Syst.*, vol. 14, no. 1, pp. 158–165, Feb. 1999.

[25] A. de la Villa Jaen, E. Acha, and A. G. Exposito, "Voltage source converter modeling for power system state estimation: STATCOM and VSC-HVDC," *IEEE Trans. Power Syst.*, vol. 23, no. 4, pp. 1552–1559, Nov. 2008.

[26] A. Benslimane, J. Bouchnaif, M. Essoufi, B. Hajji, and L. el Idrissi, "Comparative study of semiconductor power losses between CSI-based STATCOM and VSI-based STATCOM, both used for unbalance compensation," *Protection Control Mod. Power Syst.*, vol. 5, no. 1, pp. 1–14, Dec. 2020.

[27] E. Rahimi, "Commutation failure in single- and multi-infeed HVDC systems," in *Proc. 8th IEE Int. Conf. AC DC Power Transmiss. (ACDC)*, May 2006, pp. 182–186.

QUAN TANG is currently with the State Grid Sichuan Economic Research Institute, Chengdu, China.

YUNLING WANG received the M.A.Eng. degree from the Huazhong University of Science and Technology, Wuhan, China, in 2007. He is currently working as the Manager with the State Grid Sichuan Economic Research Institute. He is also involved in research on the power system planning.

CHUAN YUAN is currently with the State Grid Sichuan Electrical Power Company, Chengdu, China.

YUNKAI LEI (Member, IEEE) received the Ph.D. degree in electrical engineering from Tianjin University, Tianjin, China, in 2018. He is currently working as the Grid Planner with the State Grid Sichuan Economic Research Institute. His research interests include reliability and risk assessments of power systems and the integrated energy systems.

TING LI received the B.A. degree from Chongqing University, Chongqing, China, in 2001. She is currently working as an Executive Manager with the State Grid Sichuan Economic Research Institute. Her research interest includes the power system planning and operation.

XIAOXI YANG received the Ph.D. degree in management science and engineering from Tianjin University, China, in 2019.

She is currently a Lecturer with the College of Economics and Management, Southwest Petroleum University, China. She is also involved in research on the reliability of energy service systems.

YANG LIU (Member, IEEE) received the B.E. and Ph.D. degrees in electrical engineering from the South China University of Technology (SCUT), Guangzhou, China, in 2012 and 2017, respectively. He is currently a Lecturer with the School of Electric Power Engineering, SCUT. He has authored or coauthored more than 30 peer-reviewed SCI journal articles. His research interests include the areas of power system stability analysis and control, control of wind power generation systems, and nonlinear control theory.

• • •